ACS APPLIED BIO MATERIALS

www.acsabm.org Article

Poly-L-lysine-Functionalized Green-Light-Emitting Carbon Dots as a Fluorescence Turn-on Sensor for Ultrasensitive Detection of Endotoxin

Meenakshi Thakur and Abhijit Dan*

Cite This: *ACS Appl. Bio Mater.* 2021, 4, 3410−3422 Read Online

ACCESS | Metrics & More | Article Recommendations | Supporting Information

ABSTRACT: Herein, we report a facile, ultrasensitive, and selective fluorescence turn-on sensing strategy based on green-light-emitting functional nanodots for the detection of bacterial lipopolysaccharide (LPS) endotoxin. In this protocol, first, the pure carbon dots (CDs) with a fairly high quantum yield were prepared by microwave-assisted pyrolysis of citric acid in the presence of urea. Subsequently, the carboxyl-group-rich surfaces of the CDs were allowed to conjugate with the poly-L-lysine (PLL) using an EDC−NHS amidization method to obtain the PLL-modified CDs (PLL-CDs). The LPS could specifically bind to the PLL at the PLL−CD surfaces, and this binding enabled an electron transfer from the phosphate groups of LPS to the carbon core through the PLL bridge, thus resulting in a fluorescence enhancement. Interestingly, this fluorescent turn-on sensor provided a detection limit of 68.3 fM in PBS (pH 7.4), which is the lowest ever reported among all of the synthetic assays for LPS detection. Furthermore, our fluorescent probe was able to show a remarkable selectivity toward LPS over a range of commonly known interfering substances. Thus, this study demonstrated the feasibility of using specific LPS binding to PLL to drive molecular recognition in aqueous medium and offered an effective fluorescence turn-on sensing strategy to detect bacterial endotoxin in diverse clinical and biological applications.

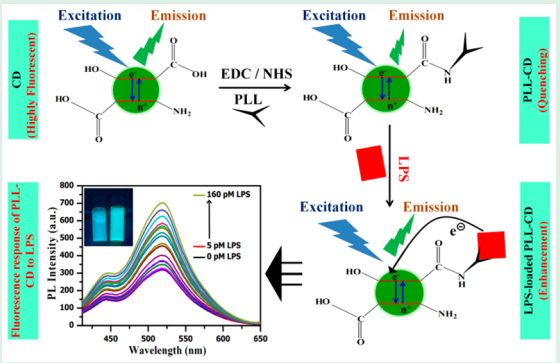

KEYWORDS: *poly-L-lysine, carbon dots, specific binding, fluorescence turn-on, LPS biosensor, ultrasensitive detection*

1. INTRODUCTION

Endotoxins, the major constituents in the outer cell membrane of Gram-negative bacteria, are directly associated with endotoximia, which can lead to septic shock and many other health diseases.[1−6] It is a lipopolysaccharide (LPS) composed of three structural units such as O-antigen, core polysaccharide, and glycophospholipid (called lipid A) (Figure 1a).[7,8] A large amount of this molecule is continuously shed into the environment during the proliferation, division, and death of bacterial cells, thereby making the lipid available for detection.[1−6] Endotoxin is an indicator of bacterial contamination, and when it enters into the bloodstream, the immune systems respond to endotoxin even in a very small quantity. For intravenous applications, the threshold endotoxin level is set to 5 endotoxin units (EU) per kilogram of body mass per hour (1 EU = 0.1−0.2 ng).[9] Therefore, detection and quantification of bacterial LPS are important in clinical and basic biomedical research,[10,11] public and occupational health,[12,13] and device and agent safety.[14,15]

The most widely used method to determine the presence of endotoxin is the so-called limulus amoebocyte lysate (LAL) assay, which employs a labile mixture of enzymes obtained from the blood of horseshoe crabs.[1] However, the complexity and variation in activity of the LAL enzyme mixtures that result from numerous interfering compounds[7,16] (including synthetic surfactants, chelating agents, divalent cations, and lipids) as well as changes in experimental conditions, particularly pH and temperature,[17,18] leads to semiquantitative results. Numerous research efforts have been devoted to achieving an improved method for endotoxin detection. Of particular recent interest in this context, the synthetic LPS biosensing assays have drawn particular attention as a promising approach due to simple methods of preparation and high sensitivity. A functionalized polydiacetylene liposome was the first reported synthetic sensor for LPS that showed a detection limit of 100 μM.[19] Another LPS-binding domain-derivative sensor was developed, enabling LPS detection as low as nanomolar concentrations.[20] LPS detection in the nanomolar range was also possible with the lipophilic pyrene derivatives.[21] Subsequently, yet another peptide-functionalized polydiacetylene (PDA) liposome-based

Received: January 4, 2021
Accepted: March 2, 2021
Published: March 12, 2021

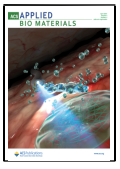

https://dx.doi.org/10.1021/acsabm.1c00006
ACS Appl. Bio Mater. 2021, 4, 3410−3422

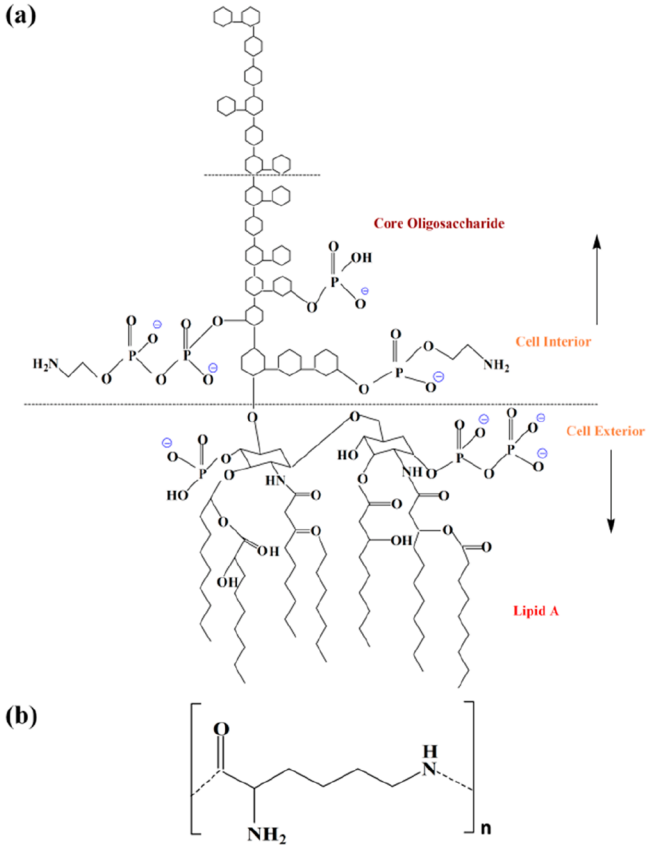

Figure 1. Chemical structure of (a) bacterial endotoxin (LPS) and (b) poly-L-lysine (PLL).

fluorescent biosensor was designed for the detection of LPS.[22] In recent years, several fluorescent, colorimetric, and surface plasmon resonance sensors based on small colloidal particles, such as copolythiophene,[23] functionalized gold, silver, platinum or Fe_3O_4 nanoparticles,[24−26] LPS-binding peptide-assembled fluorescent probes,[18,27,28] and aptamer−graphene oxide conjugates,[29,30] have been reported in the literature for sensitive detection of LPS. Although these synthetic assays have shown significant improvement of their individual detection limit ranging between nanomolar and picomolar concentrations, the current methods with their complicated fabrications and requirement of expensive instrumentation are still not robust and efficient enough for ultrasensitive detection of LPS down to a subpicomolar or femtomolar regime. Given the clinical importance of LPS, continued research effort is required toward the development of more promising materials that can offer a simple and specific sensing strategy with an ultralow detection limit.

Recently, carbon dots (CDs) have attracted particular attention as promising materials for bioimaging and biological sensing due to their strong fluorescence, water solubility, low photobleaching tendency, easy functionalization, nontoxicity, and excellent biocompatibility.[31−33] The excellent fluorescence property allows the CDs to be used as fluorescent labels, making them promising nanomaterials for specific biological applications. A number of studies have been reported using the CD labels to detect many substances such as metal ions,[34] DNA,[35] and thrombin.[36] Moreover, CDs can be attached to metal oxides,[37] polymers,[38] silica nanoparticles,[39] and graphene oxide nanosheets[40] to construct fluorescent nanohybrids with multiple functionalities. The strong fluorescence of CDs is related to the surface defect-derived origin, which induces electron−hole pair recombination.[41] Thus, a high quantum yield of CDs can be achieved by surface passivation[42] and doping with elements such as nitrogen,[43] phosphorus, sulfur,[44,45] and gadolinium.[45,46] The effective doping and surface attachment of certain active species stabilize the surface defects in the CDs with a favorable electron−hole pair recombination, resulting in a fluorescence enhancement.[47]

Poly-L-lysine (PLL), an extensively investigated linear polyelectrolyte, has been used to surface functionalize a number of materials for cellular adhesion and drug delivery applications.[48,49] In addition, PLL has been shown to possess excellent properties, including functional versatility, biodegradability, and low cytotoxicity.[50,51] The multiple aminobutyl groups in PLL impart both a positive charge of the primary amines ($-NH_3^+$) and a hydrophobic characteristic of the butyl spacer between the primary amines (Figure 1b), making this polyelectrolyte unique in its chemical behavior. Most importantly, PLL is known to specifically bind with endotoxin via both ionic and hydrophobic interactions.[52−54] This specific binding as the primary driving force for molecular recognition along with other advantageous properties allow us to combine the PLL with CDs forming a fluorescent probe for LPS detection. In particular, the combination of PLL as LPS receptor and CDs as fluorescent labels exhibits great potential to develop a novel LPS biosensor. Nevertheless, to the best of our knowledge, such synthetic assay format (CD-labeled PLL receptor) has not been explored yet in the literature.

We therefore sought to explore the opportunity to exploit the specific LPS binding to the PLL for detection of bacterial LPS. In this work, a biosensing platform using a green-light-emitting CD-labeled receptor was designed for the LPS detection based on the specific binding-triggered fluorescence turn-on strategy. Specifically, the CDs were first prepared by microwave-assisted pyrolysis of citric acid and urea, and then the carboxyl-group-rich surfaces of the CDs were conjugated with PLL using an amidization method in the presence of 1-ethyl-3-(3-dimethylaminopropyl) carbodiimide (EDC) and *N*-hydroxysucciniimde (NHS) to construct the PLL-modified CDs (PLL-CDs). In the sensing process, the LPS complexation at the PLL-CD surfaces enabled an electron transfer from the LPS to the carbon core through a PLL bridge, leading to fluorescence enhancement. We found that the developed fluorescent probe offered highly sensitive LPS detection, down to the femtomolar concentration. Moreover, LPS sensing in the presence of a number of coexisting interferents revealed that our assay was capable of showing remarkable selectivity toward LPS. Thus, this specific LPS-binding-triggered fluorescence turn-on approach provided considerable promise for bacterial endotoxin detection in clinical and biomedical relevancies.

2. EXPERIMENTAL SECTION

2.1. Materials. Citric acid was purchased from Fisher-Scientific. Urea, sodium citrate, and glucose were purchased from CDH, India. 1-Ethyl-3-(3-dimethylaminopropyl) carbodiimide (EDC) and *N*-hydroxysucciniimde (NHS) were purchased from Alfa-Aesar. Poly-L-lysine hydrobromide (PLL), lipopolysaccharide (LPS, molecular weight = 10 kDa), sodium dodecyl sulfates (SDS), cetyltrimethyammonium bromide (CTAB), dodecyl tetraethylene glycol ether ($C_{12}E_4$), bovine serum albumin (BSA), and quinine sulfate (QS) were obtained from Sigma-Aldrich. Ethylenediamine tetraacetic acid (EDTA), sodium chloride (NaCl), magnesium chloride ($MgCl_2$), and

https://dx.doi.org/10.1021/acsabm.1c00006
ACS Appl. Bio Mater. 2021, 4, 3410−3422

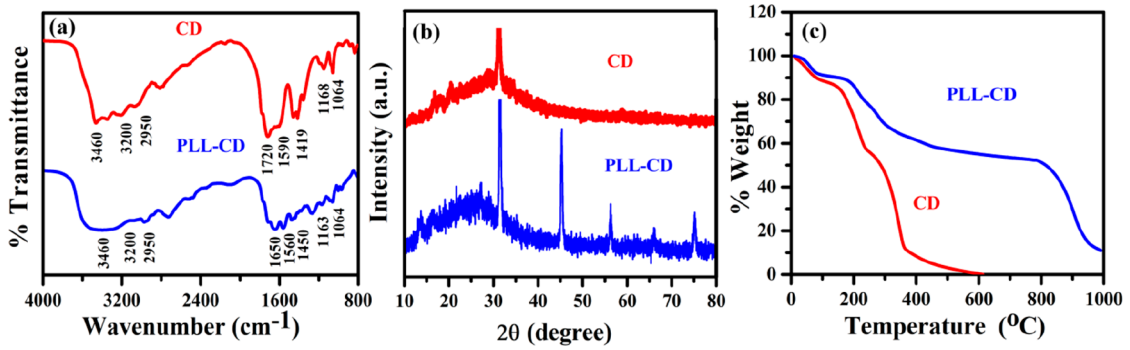

Figure 2. (a) FTIR, (b) XRD, and (c) TGA thermogram of CDs and PLL-CDs.

calcium chloride ($CaCl_2$) were purchased from Merck, India. Sodium phosphate (Na_3PO_4) was obtained from SRL, India. Phosphatidylcholine lipid was purchased from PHOSPHOLIPON. Milli-Q water (resistivity = 18.2 MΩ cm at 25 °C) was used to prepare the solutions.

2.2. Preparation of Native Carbon Dots (CDs). CDs were prepared by microwave treatment of citric acid in the presence of urea as reported elsewhere.[55] Briefly, 0.5 g of citric acid and 5 g of urea were dissolved in 10 mL of Milli-Q water and then ultrasonicated at 100 W for 5 min. The reaction mixture was placed in a 100 mL beaker and heated at 800 W in a microwave oven (IFB, 20PG4S) for 3 min. During microwave irradiation, a dark green solid was formed. After cooling down to room temperature, the solid was dispersed in 10 mL of Milli-Q water. The resulting green-colored solution was then centrifuged at 14 000 rpm for 40 min to remove the large particles. The clear greenish supernatant was collected and lyophilized for storing. The freeze-dried CDs were redispersed for further studies.

2.3. Preparation of Poly-L-lysine-Modified CDs (PLL-CDs). The PLL was functionalized on carboxyl-rich CD surfaces via EDC/NHS coupling. As described in the literature,[56] 1 mg of CDs was dispersed with EDC (75 mM) and NHS (15 mM) in 10 mL of PBS buffer (0.1 M, pH 7.4), and stirred in the dark for 1 h. Then 1 mg of PLL dissolved in 1 mL of PBS was added to the proceeding solution with simultaneous addition of 2 mL of 0.2 M NaCl. The reaction mixture was incubated with constant stirring for 2 h. Addition of NaCl was essential to reduce the electrostatic repulsions between the amino groups of the functional CDs during the reaction. Finally, the solution was dialyzed (1 kDa MWCO) to remove the unreacted species. The purified solution was lyophilized for storing.

2.4. Characterization. The prepared nanodots were characterized by various physical methods, viz., Fourier transform infrared spectroscopy (FTIR), X-ray diffraction (XRD), thermogravimetric analysis (TGA), X-ray photoelectron spectroscopy (XPS), proton nuclear magnetic resonance (^{1}H NMR), transmission electron microscopy (TEM), and dynamic light scattering (DLS). A Thermo Fisher Scientific Nicolet iS50 instrument was used to record the FTIR spectra in the range of 500−4000 cm^{-1}. The powder XRD studies were conducted on a PANalycital X'Pert PRO diffractometer at a 8 °C/min scanning rate with Cu Kα radiation (λ = 1.5418 Å) in the temperature range of 0−80 °C. The thermal stability of the samples was determined using a SDT-Q-600 TGA instrument, and the analysis was performed in the temperature range of 0−1000 °C at a heating rate of 10 °C/min under a N_2 atmosphere. For detailed elemental analysis, the XPS experiments were performed on a Thermo Fisher Scientific Nexsa system. ^{1}H NMR was conducted on a Bruker Advance NEO 500 MHz NMR spectrometer. The lyophilized CDs or PLL-CDs were redispersed in deuterated DMSO for sample preparation. The chemical shifts were measured using tetramethylsilane (TMS) as the initial standard. TEM measurements were carried out with a JEM-2100Plus (JEOL) microscope. To avoid particle aggregation, the sample solutions were ultrasonicated for 12 h prior to the measurements. The DLS experiments were carried out using a Malvern instrument (Zetasizer Nano S90). The ζ potentials of the materials at different pH values were determined using a Malvern Panalytical (Zetasizer Nano ZS) system. The absorbance spectra were collected on a Thermo Fisher Scientific (Genesys 180) UV−vis spectrophotometer. Fluorescence spectra were recorded on a PerkinElmer LS-55 spectrometer with a slit width of 10 nm for both excitation and emission.

2.5. Quantum Yield (QY) Measurements. The QY_S of CDs and PLL-CDs were determined according to the described comparative procedure using quinine sulfate (QS) as the reference standard.[41] The QS solution was prepared in 0.1 M H_2SO_4 (QY = 54%). The absorbances of QS, CD, and PLL-CD solutions were kept below 0.1. Their fluorescence spectra were recorded at the same excitation wavelength. The QY_S of the unknown samples were calculated by means of the integrated photoluminescence (PL) intensities and corresponding absorbances using the following equation

$$QY_S = QY_{QS}\left(\frac{m_S}{m_{QS}}\right)\left(\frac{\eta_S^2}{\eta_{QS}^2}\right) \quad (1)$$

where the subscripts QS and S represent the reference compound and the sample, respectively, m is the slope obtained from a linear plot of the integrated fluorescence intensity vs absorbance (0.01−0.1), and η is the refractive index of the solvent (water, η = 1.33).

2.6. Detection of LPS. For sensing experiments, LPS stock solutions of different concentrations (10 μM, 1 μM, and 100 nM) were prepared in Milli-Q water. Prior to further dilution, the LPS stock solutions were vortexed and incubated at 37 °C to avoid any aggregates formation. The LPS of different concentrations were added to the solution of PLL-CDs or CDs (5 μg/mL in PBS, pH 7.4), vortexed for 30 min, and incubated at 37 °C for 2 h. The fluorescence emission spectra of each sample were recorded at 520 nm with an excitation wavelength of 390 nm. To perform the experiments at different pH values, the samples were prepared in Milli-Q water and the pH was adjusted by adding 0.1 M HCl or 0.1 M NaOH to the solutions. In order to study the interference effect of the potential interfering agents on PLL-CD probe, the LPS-spiked samples (160 pM) were prepared in the presence of different interfering compounds. Then the PL intensities of the LPS-spiked samples were recorded and compared with those of nonspiked samples.

2.7. Bacterial Assays. The *E. coli* (0157:H7) cells were cultivated in the nutrient broth media. The culture was allowed to grow overnight at 37 °C until the absorbance at 600 nm (OD_{600}) reached 1.0. An optical density of 1.0 at 600 nm corresponded to ~8.8×10^8 cells/mL. The cell mixture was centrifuged at 7800 rpm for 10 min and washed twice with PBS buffer. The bacterial cells were resuspended in PBS buffer and diluted to final concentrations ranging between 5.1×10^6 and 3.8×10^8 cells/mL. The OD_{600} of each sample was measured. The bacterial cell concentration was determined using a standard calibration curve. Prior to the fluorescence measurement, the diluted cells were incubated with the PLL-CDs at 37 °C for 2 h under gentle shaking.

https://dx.doi.org/10.1021/acsabm.1c00006
ACS Appl. Bio Mater. 2021, 4, 3410−3422

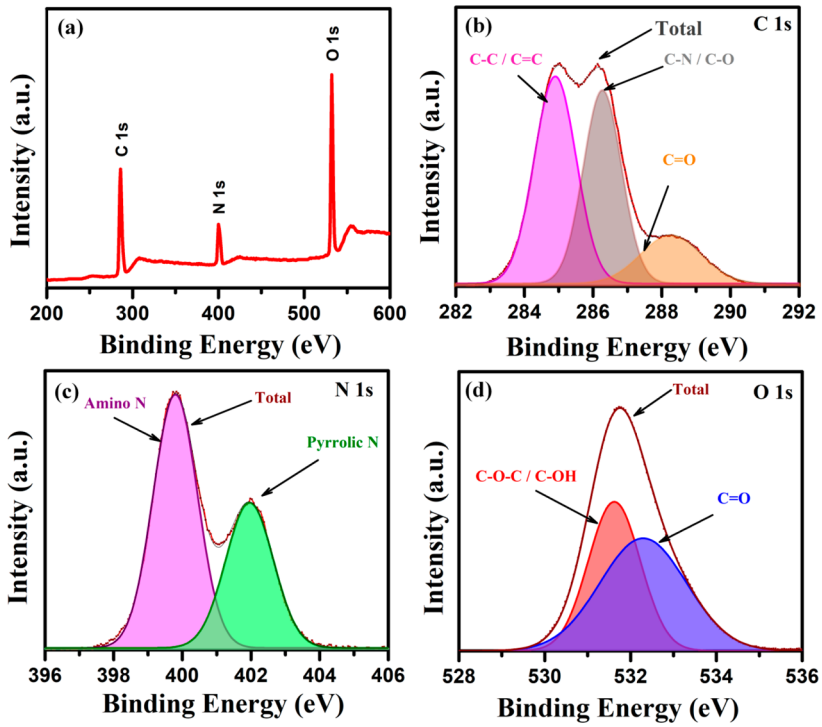

Figure 3. (a) XPS full-scan survey and deconvoluted high-resolution XPS spectra of (b) C 1s, (c) N 1s, and (d) O 1s of PLL-CDs.

3. RESULTS AND DISCUSSION

3.1. Material Characterization. Successful functionalization of PLL on the CD surface was confirmed by FTIR spectroscopy (Figure 2a). The FTIR spectra of bare CDs exhibited two characteristic peaks at 1064 and 1720 cm^{-1} corresponding to C−O and C═O stretching vibrations of the −COOH groups, respectively. The peaks appearing at 1168 and 1590 cm^{-1} were ascribed to the C−O−C stretching vibration and C═C stretch of the sp^2 carbon skeletal network of the CDs, respectively. The absorbance bands at 1419 and 2950 cm^{-1} corresponded to the CH_2 bending and symmetric as well as asymmetric C−H stretching, respectively. The peaks appearing between 3200 and 3460 cm^{-1} were attributed to −OH and $-NH_2$ stretching, respectively. In the case of PLL-CDs, the peak corresponding to the C═O stretch of −COOH disappeared while the characteristic peaks at 1560 and 1650 cm^{-1} associated with the N−H bending and C═O stretching of the amide groups, respectively, appeared. This suggests the progress of the amidization reaction between the −COOH groups of CDs and the $-NH_2$ groups of PLL. Other characteristic peaks associated with C−O, C−O−C, C−H, O−H, and N−H stretching of PLL-CDs appeared at their respective wavenumbers as observed in case of bare CDs, indicating the presence of CDs in the functionalized materials. Thus, the PLL molecules that were covalently anchored with the CDs via amide linkage could act as receptors for bacterial LPS.

The XRD patterns of CDs and PLL-CDs are presented in Figure 2b. Both materials exhibited a broad peak at 25°, which could be assigned to the (002) plane of graphite. In addition, the sharp diffraction peaks at 28° for CDs and 31°, 45°, 56°, and 75° for PLL-CDs appeared due to the presence of disordered carbon atoms in the materials. The interlayer distances between the (002) planes of CDs and PLL-CDs were calculated by Bragg's equation to be 0.488 and 0.538 nm, respectively, larger than that of pure graphite (0.335 nm). The broad diffraction peak with a higher interlayer distance was indicative of the amorphous nature of CDs/PLL-CDs, which could be attributed to the formation of defect sites through oxygen-containing groups or/and PLL functionality in the crystal lattice. Overall, the XRD patterns suggested that the microwave-assisted synthesis of the materials led to the formation of a turbostratic carbon structure with highly disordered carbon atoms.

The thermal stability of the prepared nanodots was determined using TGA measurements. The thermograms of both CDs and PLL-CDs (Figure 2c) showed an initial weight loss of 8−10% up to ∼100 °C due to the evaporation of physiosorbed water. Consistent with the previous reports,[57,58] a two-stage degradation pattern between 160 and 330 °C was observed for CDs, suggesting the decomposition of amino- and oxygen-containg groups. The weight loss after 330 °C indicated a gradual degradation of the carbon core of CDs. A remarkable enhancement of the thermal stability was observed for PLL-CDs. The TGA thermogram of PLL-CDs exhibited a gradual weight loss in the temperature range of 160−800 °C corresponding to decomposition of the PLL functionality. The weight loss between 800 and 1000 °C was due to the degradation of unreacted functional moieties and the carbon core of PLL-CDs.

The elemental composition and chemical bonds present in the as-prepared PLL-CDs were determined using XPS measurements, and the results are presented in Figure 3. The full-scan XPS spectrum (Figure 3a) revealed the presence of carbon (C 1s), nitrogen (N 1s), and oxygen (O 1s) as the three major elements in the PLL-CDs with the characteristic peaks at 284.9, 400.5, and 531.8 eV, respectively. The high-resolution C 1s spectrum (Figure 3b) showed three major deconvoluted peaks at 284.5, 286.1, and 288.2 eV corresponding to C−C/C═C, C−N/C−O, and C═O, respectively. Similarly, the deconvoluted N 1s spectrum (Figure 3c)

https://dx.doi.org/10.1021/acsabm.1c00006
ACS Appl. Bio Mater. 2021, 4, 3410−3422

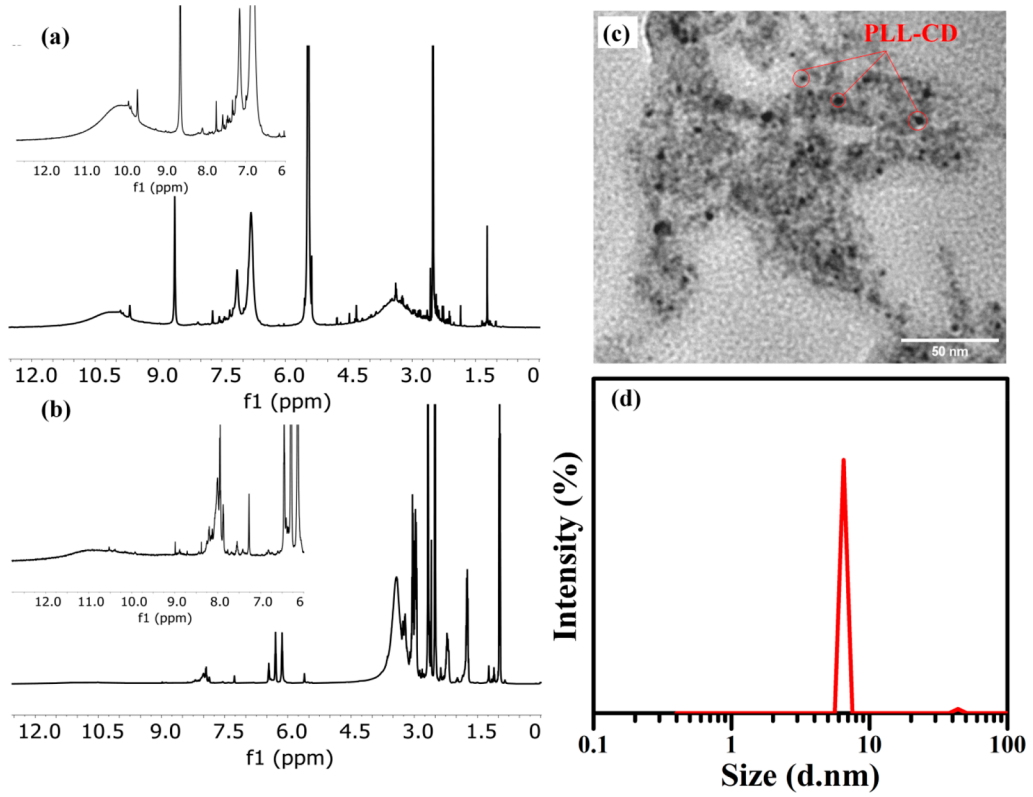

Figure 4. ^{1}H NMR spectra of (a) CDs and (b) PLL-CDs. (c) HR-TEM image and (d) particle size distribution by DLS measurement of PLL-CDs.

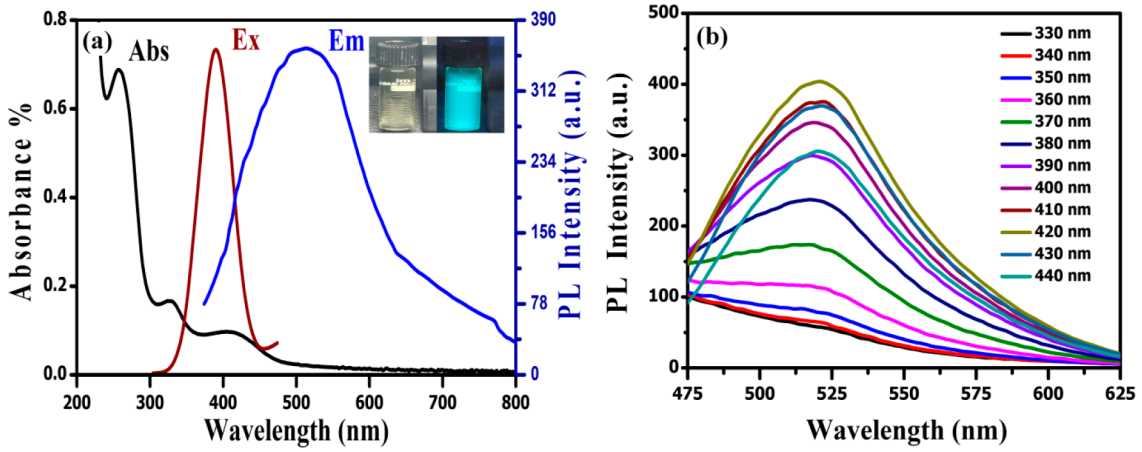

Figure 5. (a) UV−vis absorption, PL excitation at 410 nm, and PL emission at 520 nm spectra of PLL-CDs. (Inset) Photographs of aqueous PLL-CDs dispersion under normal light (left) and 365 nm UV irradiation (right). (b) PL emission spectra of PLL-CDs at different excitation wavelengths.

revealed two major nitrogen peaks at 399.8 and 401.4 eV, reflecting the presence of amino and pyrrolic N, respectively. In the deconvoluted O 1s spectrum (Figure 3d), the two main peaks with binding energies at ca. 531.6 and 532.4 eV were assigned to C−O−C/C−OH and C═O, respectively. Hence, the XPS survey of PLL-CDs is consistent with the FTIR spectra.

In order to further confirm the PLL functionalization on the CD surfaces, ^{1}H NMR analysis of CDs and PLL-CDs was carried out as presented in Figure 4a and 4b. The ^{1}H NMR spectrum of CDs (Figure 4a) was dominated by aromatic resonance peaks ranging between 6.5 and 9 ppm with an intense chemical shift at 5.45 ppm corresponding to the phenolic protons. A broad peak appearing around 10.2 ppm (Figure 4a, inset) confirmed the existence of active protons of the aromatic carboxylic groups in CDs. PLL-CDs showed a number of proton peaks in the range of 1.0−2.2 ppm (Figure 4b), indicating the presence of aliphatic hydrogens originating from the PLL functionality. Interestingly, the resonance peak associated with the protons of the aromatic carboxylic acid disappeared, while the signals in the range of 6.2−6.5 ppm corresponding to the amide protons appeared in the ^{1}H NMR spectra of PLL-CDs (Figure 4b, inset). These results suggested that the $-NH_2$ groups of PLL reacted with the −COOH groups of CDs to form the amide linkages, thus confirming the PLL functionality on the surfaces of CDs.

https://dx.doi.org/10.1021/acsabm.1c00006
ACS Appl. Bio Mater. 2021, 4, 3410−3422

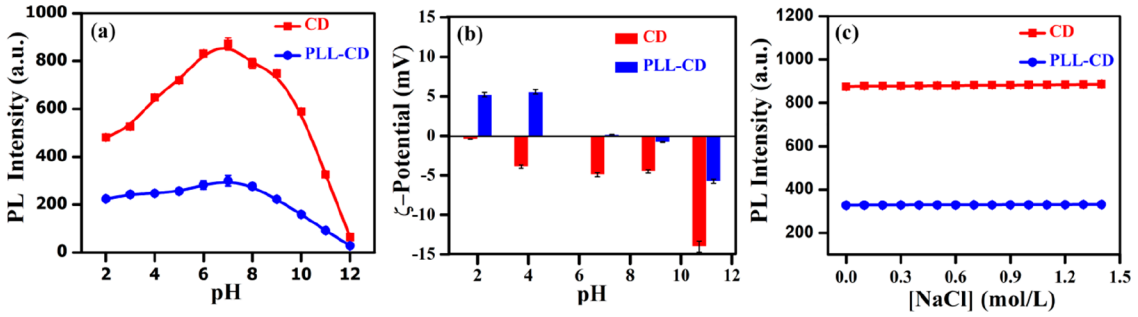

Figure 6. (a) Effect of pH on the PL emission, (b) ζ-potentials at different pH values, and (c) effect of ionic strength on PL emission of CDs and PLL-CDs.

The morphology and particle size of PLL-CDs were assessed by TEM measurements as shown in Figure 4c. It could be seen that the particles were well dispersed and exhibited a spherical shape morphology with an average particle size of ∼3.2 nm. Corresponding size distribution analysis by DLS (Figure 4d) showed a narrow size distribution. The average particle size of the PLL-CD nanodots as obtained from the DLS measurements was ∼5.6 nm. Thus, the particle size obtained from TEM study was shown to have good agreement with that measured by DLS.

The optical properties of the as-synthesized CDs and PLL-CDs were determined by UV−vis absorption and PL spectra. Figure 5a presents the UV−vis spectra, PL excitation, and emission spectra of PLL-CDs with the inset showing its pictures under different light (the optical behaviors of pure CDs are presented in Figure S1). The UV−vis spectrum of both CDs (Figure S1a) and PLL-CDs (Figure 5a) showed three absorption peaks at 258, 330, and 410 nm. Specifically, the peak arising at 258 nm was attributed to the $\pi-\pi^*$ transition of the aromatic moieties of the carbon core, while the peak at 330 nm was ascribed to the n−π^* transition of the functional groups (e.g., C═O) present on the surface of the nanodots. The absorption band at 410 nm was due to the $\pi-\pi^*$ transition of the core pyridone ring.[59,60] The aqueous dispersion of PLL-CDs was shown to be a transparent yellow solution when viewed under normal light, whereas it emitted a green luminescence under UV irradiation (inset, Figure 5a). The nanodots exhibited a maximum emission at 520 nm upon excitation at 410 nm (Figure 5a and Figure S1a).

The PL emission spectra of CDs and PLL-CDs under different excitation wavelengths ranging between 330 and 440 nm are depicted in Figure S1b and Figure 5b, respectively. The nanodots showed characteristic excitation-independent fluorescence emission as reported in a recent study for green luminescent nanodots prepared by microwave treatment of citric acid in the presence of urea.[61] The observed excitation-independent PL properties suggested a relatively uniform emission from the nanodots. Notably, the prepared nanodots were sufficiently small in size (<10 nm) with a narrow particle size distribution, and they formed a good dispersion in water; therefore, the size and solvent were expected to have no influence on the PL properties. Further, it can be seen that with increasing excitation wavelength the emission increased and reached an emission maximum at 420 nm, and then the emission intensity gradually decreased.

The QY of PLL-CDs was determined to be 3.53%, which was lower than that of pure CDs (8.42%) (Figure S2). This decrease of QY in the case of PLL-CDs was likely due to the emission quenching by polymeric loading. However, the florescence property was sufficient enough to meet the needs for quantitative determination of aqueous analytes.

The pH of the solution strongly influenced the PL properties of CDs and PLL-CDs as it changed the degree of protonation/deprotonation of the surface functional groups and thus the electron-donating efficiency of the nanodots. The inherent pH values of CDs and PLL-CDs in Milli-Q water were found to be 3.2 and 5.8, respectively. The PL intensity of CDs increased with increasing pH, reached a maximum at pH 7, and then decreased with a further increase of pH (Figure 6a and Figure S3a). The lower fluorescence intensity in acidic medium (pH < 7) might be due to the particle aggregation via hydrogen bonding between the hydroxyl and the carboxylic moieties. Thus, the CDs underwent electron exchange with each other, resulting in a decreased electron-donating efficiency.[61] At higher pH (pH > 7), the decrease of PL intensity could be explained by the extensive deprotonation of the oxygen-containing surface functional groups (−OH and −COOH) of CDs. The repulsive interaction under such condition increased the dynamic motion of the nanodots, causing friction with the solvent media. This suggested a transformation of photonic energy to thermal energy, which resulted in a radiationless relaxation of excitons,[62−65] thus reducing their PL emission.

Interestingly, PLL-CDs maintained almost the same PL property over a range of pH values from 2 to 8 with a maximum emission efficiency at pH 7 (Figure 6a and Figure S3b), implying a good PL stability of PLL-CDs. A large number of carboxyl groups of CDs were engaged in the formation of amide linkage with PLL in PLL-CDs. Therefore, the pH dependency of PLL-CD emission was mainly controlled by the protonation−deprotonation of amino groups originating from PLL or CDs, amide groups formed after functionalization, and hydroxyl groups originated from CDs. In addition, the electron availability in the carbon core of PLL-CDs decreased dramatically due to migration of electrons to the PLL chains, leading to suppression of the emission intensity as shown in Figure 6a.

The results of the ζ-potential measurements as presented in Figure 6b further explain the pH-dependent PL behaviors of CDs and PLL-CDs. The surfaces of CDs remained negatively charged within the entire pH range (pH 2−11) due to the presence of oxygen-containing functional groups (−OH and −COOH). In contrast, the PLL-CD surfaces were found to be positively charged up to pH 7.4, after which the ζ potentials became negative. The positive ζ-potential values of PLL-CDs at pH ≤ 7.4 were consistent with protonation of the amino or amido groups originating from the PLL functionality. In fact, PLL-CDs exhibited a favorable electron transport from the carbon core to the PLL chains, resulting in a reduced PL

https://dx.doi.org/10.1021/acsabm.1c00006
ACS Appl. Bio Mater. 2021, 4, 3410−3422

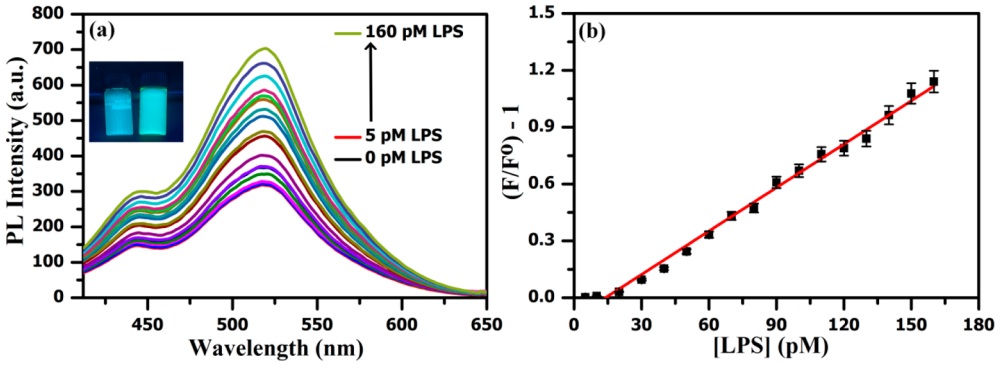

Figure 7. (a) Fluorescence titration of PLL-CDs upon addition of various concentrations of LPS in PBS buffer (pH 7.4). (Inset) Photographs of the corresponding color change without (left) and with (right) 160 pM LPS under 365 nm UV light. (b) Stern−Volmer plot of PL intensity change versus LPS concentration. F and $F°$ are the PL intensities at 520 nm with and without LPS, respectively.

Table 1. Analytical Parameters for Determination of LPS Using PLL-CDs

parameters	pH 7.4	pH 4	pH 9	1 M NaCl
linear dynamic range	0−160 pM	0−160 pM	0−160 pM	0−120 pM
regression equation	y = 0.0076x - 0.106	$y = 0.0088x - 0.14$	$y = 0.0051x - 0.04$	$y = 0.0083x - 0.01$
R^2	0.9917	0.9922	0.9901	0.9927
LOD (fM)	68.3	67.2	74.1	72.4
binding constant (M^{-1})	4.9×10^9	4.6×10^9	2.3×10^9	2.9×10^9

Table 2. Comparison of the LPS Detection Performance of PLL-CDs with Other Synthetic Assays

sensors	bacteria	LOD	ref
PLL-CDs	*E. coli* O157:H7	68.3 fM	present study
amino acid-functionalized polydiacetylene liposomes	*E. coli* O26:B6.	100 μM	19
CD14 peptides	*E. coli* 055:B5	150 nM	20
pyrene derivatives	*E. coli* 055:B5	100 nM	21
peptide-functionalized polydiacetylene liposomes	*E. coli* DH5α	100 μM	22
peptide-assembled GO	*E. coli* DH5α	130 pM	67
copolythiophene CPT1-C	*E. coli, K. pneumoniae*	270 pM	23
cysteamine-modified Au NPs	*E. coli* 055:B5	330 pM	24
CTAB-capped Au nanospheres	*E. coli* 055:B5	560 pM	25
polymyxin B-functionalized Ag−NPs		2 nM	26
Janus Pt−micromotors	*Salmonella enterica*	7 pM	27
$CuFeO_2$@chitosan/Fe_3O_4@chitosan	*Pseudomonas aeruginosa*	45 μM	28
peptide-functionalized Fe_3O_4@SiO_2 core−shell MNPs	*E. coli* DH5α	28 nM	18
peptide (P16)−fluorophore (CTPY) conjugates	*E. coli* 0111:B4	6.97 nM	68
aptamer−GO conjugates	*E. coli* 055:B5	1.57 nM	29
aptamer−CdSe/ZnS QD	*E. coli* 055:B5	0.87 nM	69

intensity compared to pure CDs. In alkaline condition (pH > 7.4), the hydroxyl groups originating from CDs underwent deprotonation, making the PLL-CD surfaces negatively charged.

The effect of ionic strength on the PL emission of CDs and PLL-CDs was studied in a set of NaCl solutions with different concentrations (0−1.4 M). The PL intensity of both CDs and PLL-CDs remained constant over a wide range of NaCl concentrations as shown in Figure 6c and Figure S4, suggesting that the nanodots were fairly stable against particle−particle interactions such as van der Waals forces. These results revealed that PLL-CDs had a relatively stable emission in a broad range of pH values and excellent tolerance for high ionic strength, which made them a promising candidate for fluorescence-based detection of biological analytes.

3.2. LPS Detection. The potential of PLL-CDs to determine the presence of LPS in aqueous medium was evaluated by measuring the fluorescence response of the nanodots to LPS extracted from *E. coli*. As shown in Figure 7a, introduction of LPS to the aqueous PLL-CD dispersion in PBS (pH 7.4) resulted in a remarkable enhancement of the PL intensity without a spectral shift. Furthermore, upon incremental addition of LPS from 0 to 160 pM, the PL intensity was found to gradually increase. In contrast, pure CDs did not show any significant change in the PL intensity (no enhancement or quenching) upon addition of LPS (Figure S5). These findings suggest that the specific LPS binding to PLL via electrostatic as well as hydrophobic interactions led to the formation of a complex-coated layer, which reduced the surface defects of the nanodots.[66] The fluorescence response could be easily detected by the naked eye under UV light (365 nm) at a LPS concentration of 160 pM (Figure 7a, inset).

In order to quantify the amount of LPS present in the aqueous solution, the Stern−Volmer plot of the normalized PL intensity $(F/F°) - 1$, where $F°$ is the PL intensity in the absence of LPS, versus the LPS concentration was prepared

https://dx.doi.org/10.1021/acsabm.1c00006
ACS Appl. Bio Mater. 2021, 4, 3410−3422

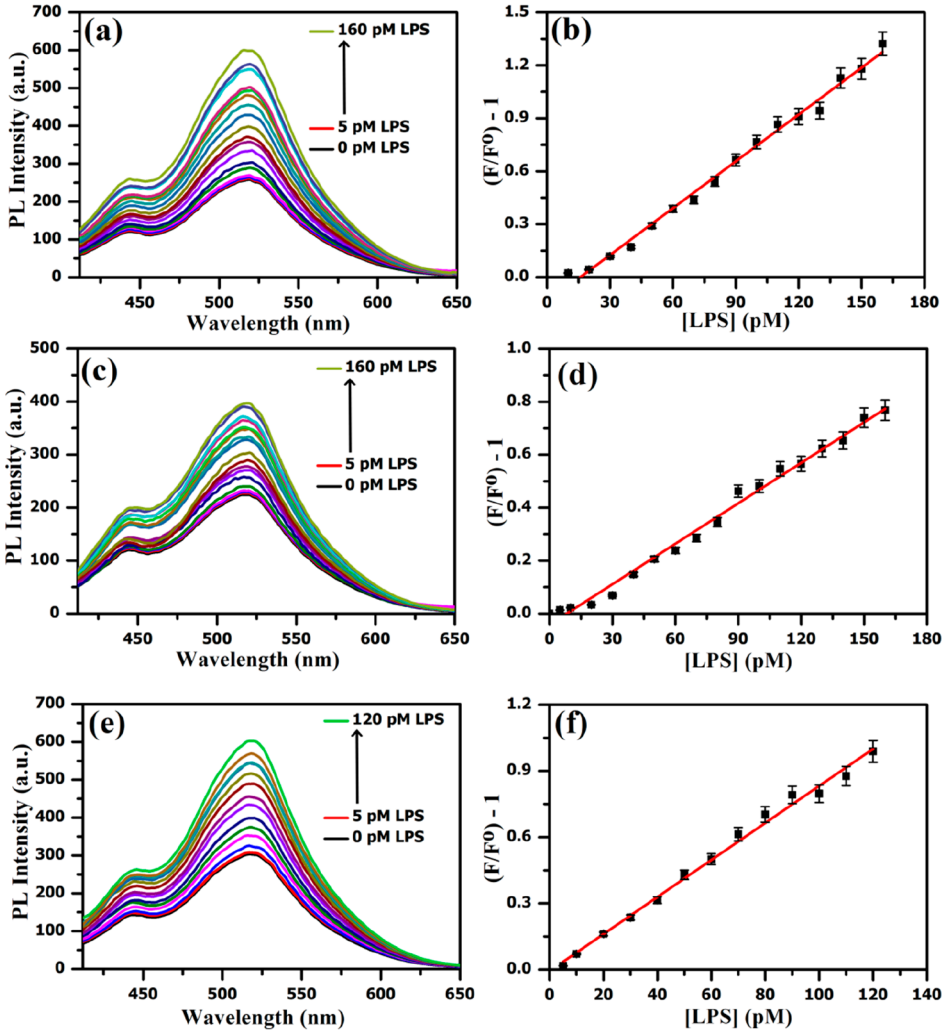

Figure 8. Fluorescence titration of PLL-CDs upon addition of different concentrations of LPS (left) at (a) pH 4 and (c) pH 9 and (e) in the presence of 1 M NaCl. Stern−Volmer plot of PL intensity change vs LPS concentration (right) at (b) pH 4 and (d) pH 9 and (f) in the presence of 1 M NaCl. F and $F°$ are PL intensities at 520 nm with and without LPS, respectively.

(Figure 7b). The corresponding analytical parameters are listed in Table 1. The curve showed a good linear relationship (correlation coefficient, R^2 = 0.9917) between the PL intensity ratio and the LPS concentration in the studied range. The limit of detection (LOD) was calculated using the standard equation, LOD = 3Q/slope, where Q is the standard deviation of blank samples. The LOD was determined to be as low as 68.3 fM. The Job's plot-based fluorescence analysis as shown in Figure S6 indicated a 1:2.3 stoichiometric binding ratio between PLL-CDs and LPS. Moreover, we compared the sensing performance of PLL-CDs toward LPS with the literature values obtained using other synthetic LPS sensors and tabulated the results in Table 2. It can be clearly seen that the LOD for PLL-CDs was at least one/two orders of magnitude lower than that of many other synthetic assays reported in the literature for LPS detection. Therefore, PLL-CDs can act as excellent cost-effective materials for ultra-sensitive detection of LPS in aqueous solution.

Furthermore, the sensing performance of the PLL-CD probe toward LPS was investigated in different solution conditions such as acidic (pH 4) and alkaline (pH 9) media and in the presence of salt (1 M NaCl). Figure 8a,c shows the PL emission spectra of PLL-CDs in the presence of different LPS concentrations at pH 4 and 9, respectively. The good linear relationships between the PL intensity ratio and the LPS concentrations were recorded at both pH values of the solutions (Figure 8b and 8d). The corresponding analytical performance data are tabulated in Table 1. In acidic medium (pH 4), the LOD (67.2 fM) was found to be a little lower than that of other studied solution conditions. At lower pH, the amino or amido groups of PLL in PLL-CDs could be easily protonated, consistent with the positive ζ-potential values (Figure 6b), leading to a favorable electrostatic interaction with the negatively charged LPS in addition to hydrophobic interaction. This suggested a strong LPS binding at the surface of PLL-CDs, which induced a large fluorescence enhancement. In contrast, the PLL-CDs possessed negative ζ-potentials at high pH (Figure 6b), and hence, the LPS molecules experienced difficulty to occupy the surface sites of PLL-CDs due to electrostatic repulsion, resulting in a relatively less pronounced fluorescence enhancement. The PL intensity enhancement in this case was attributed to the LPS complexation via hydrophobic interaction only. The LPS sensing performance of PLL-CDs was also evaluated at a fairly high ionic strength. In the presence of 1 M NaCl, the PLL-CDs provided a similar fluorescence response (Figure 8e) with a

https://dx.doi.org/10.1021/acsabm.1c00006
ACS Appl. Bio Mater. 2021, 4, 3410−3422

Scheme 1. Formation of PLL-CDs and Its Working Principle for Fluorescence Turn-on Detection of LPS

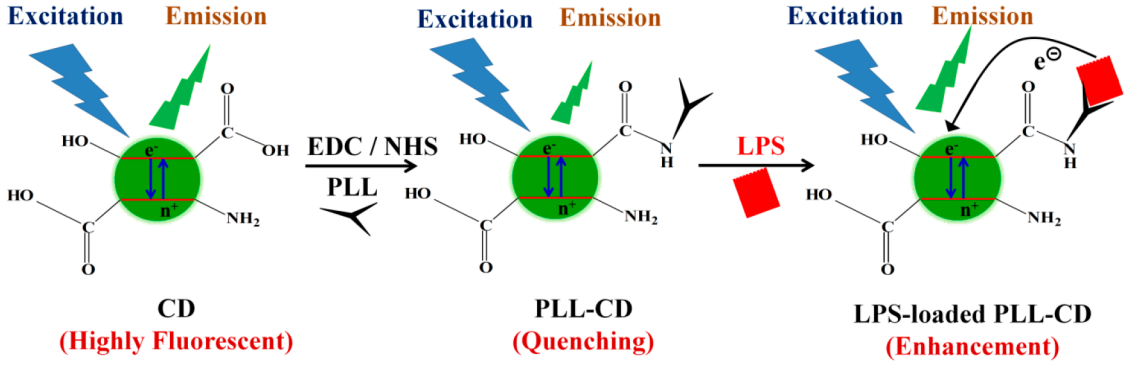

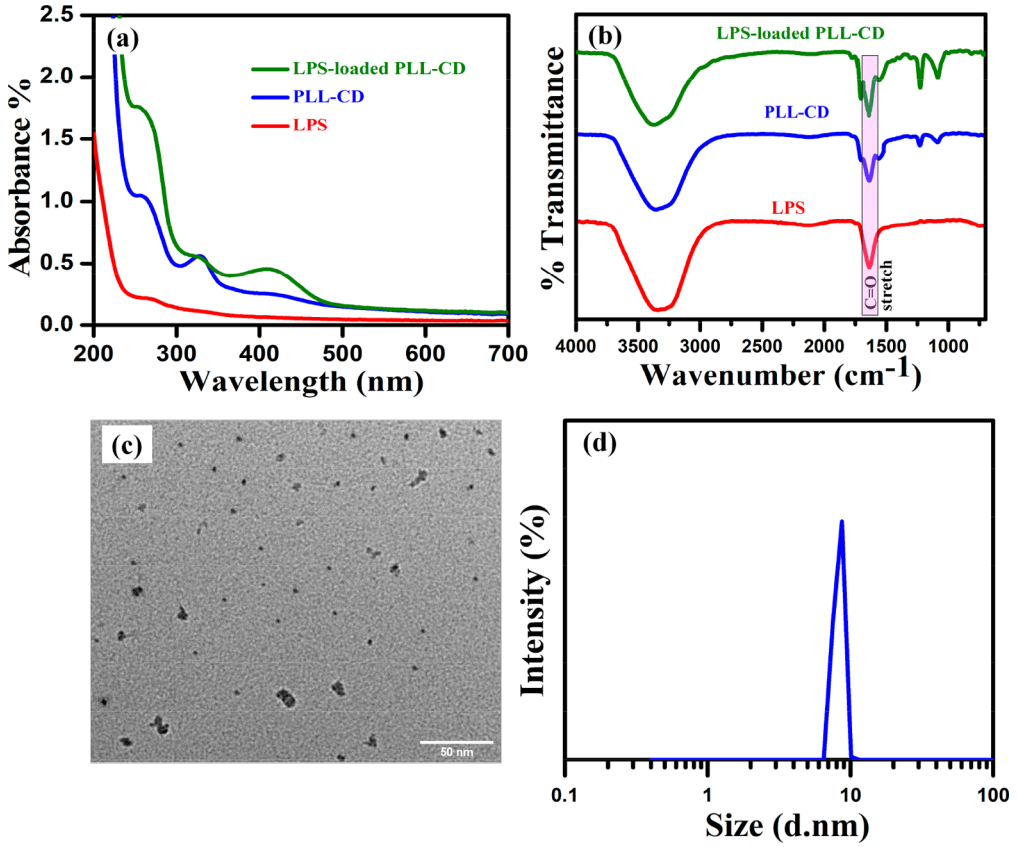

Figure 9. (a) UV−vis and (b) FTIR spectra of LPS, PLL-CDs, and LPS-loaded PLL-CDs. (c) HR-TEM image and (d) particle size distribution by DLS measurement of LPS-loaded PLL-CDs.

good linear relationship (Figure 8f) as in LPS-spiked PBS buffer, suggesting an excellent tolerance for high ionic strength. The binding constants of PLL-CDs toward LPS in neutral (pH 7.4), acidic (pH 4), and alkaline (pH 9) conditions and in the presence of 1 M NaCl were calculated using a Benesi−Hildebrand plot (Figure S7) to be 4.9×10^9, 4.6×10^9, 2.3×10^9, and 2.9×10^9 M^{-1}, respectively (Table 1).

The mechanistic insight underlying the fluorescence turn on of PLL-CDs and the role of PLL in the sensing of LPS are demonstrated on the basis of the electron transfer effect as shown in Scheme 1. We hypothesized that the LPS was attached to the surface of PLL-CDs as the LPS is known to bind specifically to the PLL via both ionic and hydrophobic interactions, particularly at pH $\leq$ 7.4.[52] This complex formation at the particle surface that induced an electron transfer from the phosphate groups of LPS to the carbon core through the PLL bridge was the principle behind the fluorescence turn-on sensing of LPS. The migration of electrons might reduce the surface defects of the nanodots. This led to an effortless electron−hole pair recombination, thus resulting in an enhancement of the fluorescence intensity.[70] On the contrary, the LPS experienced a repulsive interaction by the deprotonated oxygen-containing groups of PLL-CDs at higher pH (i.e., pH > 7.4), which in turn made the LPS binding weak. Only the hydrophobic interaction contributed to the binding between LPS and PLL, and hence, electron transfer was less effective in alkaline condition.

In support of the proposed mechanism as described above, complex formation at the particle surface was evaluated by ζ-potential, UV−vis, and FTIR spectra. Addition of LPS resulted in a change of the ζ-potential value of aqueous PLL-CDs dispersion from +0.167 to −2.63 mV at pH 7.4. The UV−vis

https://dx.doi.org/10.1021/acsabm.1c00006
ACS Appl. Bio Mater. 2021, 4, 3410−3422

spectra presented in Figure 9a revealed that the intensities of the absorption bands at 258 and 410 nm associated with the $\pi-\pi^*$ transitions of the core aromatic moieties of PLL-CDs significantly increased after addition of LPS. The FTIR study (Figure 9b) of the aqueous dispersion of LPS, PLL-CDs, and LPS-loaded PLL-CDs provided further evidence of successful attachment of LPS on the PLL-CD surfaces. Furthermore, the size and morphology of the LPS-loaded PLL-CD conjugates was characterized by TEM and DLS measurements. Interestingly, the size of the nanodots remained more or less the same (~3.7 nm) after LPS complexation as observed in the TEM image (Figure 9c) of PLL-CDs in the presence of 160 pM LPS. In agreement with the TEM results, the DLS data (Figure 9d) shows that the average particle size of the LPS-loaded PLL-CDs was ~7.4 nm. These findings confirmed that the complex formation between LPS and PLL at the PLL-CD surfaces induced an electron transfer from the LPS to the carbon core, resulting in a fluorescence enhancement.

3.3. Selectivity. The selectivity of the prepared fluorescent sensor was evaluated by monitoring the fluorescence response of the PLL-CDs to a number of coexisting species that are known to interfere with the LAL assay such as surfactants (anionic SDS, cationic CTAB, and nonionic $C_{12}E_4$), lipid (phosphatidylcholine), chelating agents (EDTA and citrate), divalent cations (Mg^{2+} and Ca^{+2}), protein (BSA), and functional groups found in LPS (phosphate, glucose, starch, and O-antigen). We found that the interfering substances at relatively high concentrations (1 mg/mL for BSA and 10 μM for other compounds) hardly altered the PL intensity of PLL-CDs (no enhancement or quenching) as shown in Figure 10 (red bars), indicating a limited influence of the interferents on the probe. The exclusive response to LPS could be explained by the obvious selective binding of LPS to PLL at the PLL-CD surfaces. Interestingly, a significant enhancement of the fluorescence emission of the PLL-CDs was observed on subsequent addition of LPS (160 pM) to all of the above systems (Figure 10, blue bars). However, in the presence of these interfering compounds, our fluorescent probe exhibited minimal false positives or negatives with very small enhancement/inhibition of the fluorescence turn-on-based biosensing of LPS. These results confirmed the excellent selectivity of the PLL-CDs toward LPS, even in the presence of potential interfering compounds.

3.4. Detection of Living *E. coli* Cells. To determine the potential of this fluorescent probe in practical applications, we further extended our study for the detection of living *E. coli* cells. As shown in Figure 10b, the PL intensity gradually increased with increasing *E. coli* cell concentration, suggesting that similar to LPS, the *E. coli* cells were able to induce a fluorescence enhancement of PLL-CDs. In the high-concentration regime (e.g., 3.8×10^8 cells/mL), the response was clearly visible under illumination from a UV lamp (Figure 10b, inset I). The fluorescence signal exhibited a good linear relationship (R^2 = 0.9824) with *E. coli* concentration ranging from 5.1×10^6 to 3.4×10^8 cells/mL (Figure 10b, inset II). Thus, the PLL-CD probe with excellent sensing performance offers great promise to detect living bacterial cells in clinical and biological relevance.

4. CONCLUSIONS

We demonstrated a facile design and synthesis of PLL-functionalized green-light-emitting CDs (PLL-CDs), which can act as a robust fluorescence turn-on sensor for selective and ultrasensitive detection of bacterial endotoxin (LPS). This approach involved the preparation of pure CDs from citric acid precursor in the presence of urea by microwave-assisted pyrolysis followed by the attachment of PLL on the carboxyl-group-rich surface of the CDs through EDC/NHS coupling. The LPS binding to PLL at the PLL-CD surfaces induced an electron transfer from the phosphate groups of LPS to the carbon core through the PLL bridge, resulting in an enhancement of the PL intensity. The PLL-CDs exhibited a linear relationship between the PL intensity change ratio and the LPS concentration in the studied region (0–160 pM), enabling the quantitative determination of the LPS. Interestingly, the LOD was found to be 68.3 fM in PBS buffer (pH 7.4), which is the lowest among all of the synthetic assays reported for LPS detection to date. Moreover, our results revealed that this fluorescent probe was shown to have excellent sensing performance toward LPS in a range of solution conditions including different pH values and ionic

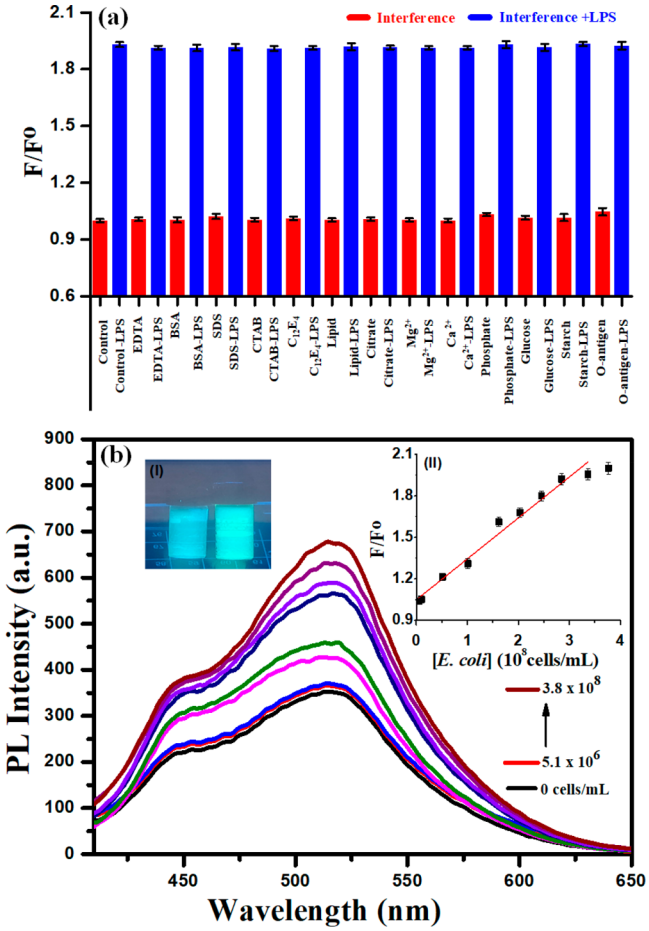

Figure 10. (a) Fluorescence responses of the PLL-CDs to various potential coexisting interferents. Red bars represent the change in the PL intensity ratio (F/F°) upon addition of interferents (1 mg/mL for BSA and 10 μM for other compounds) to the probe. Blue bars represent the change in the PL intensity ratio upon addition of 160 pM LPS to the solutions in the presence of interferents. (b) Fluorescence titration of PLL-CDs upon addition of various concentrations of living *E. coli* cells in PBS (pH 7.4). (Inset I) Photographs of the corresponding color change without (left) and with (right) 3.8×10^8 cells/mL *E. coli* under 365 nm UV irradiation. (Inset II) Plot of PL intensity ratio (F/F°) versus *E. coli* concentration. F and F° are the PL intensities at 520 nm with and without LPS or *E. coli*, respectively.

https://dx.doi.org/10.1021/acsabm.1c00006
ACS Appl. Bio Mater. 2021, 4, 3410–3422

strengths. This probe was specific for LPS, and thus, it allowed selective detection of LPS over a range of potential coexisting interferents. The assay format could also be used to detect living *E. coli* cells. Overall, this specific LPS-binding-triggered fluorescence turn-on strategy provided a promising platform for the development of LPS biosensors, thus offering great potential for the detection of bacterial endotoxin in biological samples, medical devices, and pharmaceutical products.

■ ASSOCIATED CONTENT

Supporting Information

The Supporting Information is available free of charge at https://pubs.acs.org/doi/10.1021/acsabm.1c00006.

UV−vis and PL spectra of CDs; integrated PL intensity vs absorbance plot for QY measurements; PL intensity of CDs and PLL-CDs at different pH; PL intensity of CDs and PLL-CDs at different ionic strengths; PL intensity of CDs as a function of LPS concentration; Job's plot for determination of the stoichiometric binding between PLL-CDs and LPS; Benesi−Hildebrand plot for determination of the binding constant (PDF)

■ AUTHOR INFORMATION

Corresponding Author

Abhijit Dan − *Department of Chemistry and Centre for Advanced Studies in Chemistry, Panjab University − Chandigarh, Chandigarh 160014, India;* orcid.org/0000-0002-7656-3956; Email: abhijit@pu.ac.in

Author

Meenakshi Thakur − *Department of Chemistry and Centre for Advanced Studies in Chemistry, Panjab University − Chandigarh, Chandigarh 160014, India*

Complete contact information is available at: https://pubs.acs.org/10.1021/acsabm.1c00006

Author Contributions

A.D. designed the research and contributed to analysis of the data. M.T. performed the experiments and analyzed the data. A.D. wrote the manuscript with M.T.

Notes

The authors declare no competing financial interest.

■ ACKNOWLEDGMENTS

A.D. gratefully acknowledges the financial support received from the DST Ramanujan fellowship scheme (SB/S2/RJN-119/2015) and UGC start-up grant (F.4-5(244-FRP)/2015/BSR). M.T. acknowledges DST, India for the INSPIRE fellowship.

■ REFERENCES

(1) Raetz, C. R. H.; Whitfield, C. Lipopolysaccharide Endotoxins. *Annu. Rev. Biochem.* **2002**, *71*, 635−700.

(2) Ma, R.; Zhao, J.; Du, H.; Tian, S.; Li, L. Removing Endotoxin from Plasmid Samples by Triton X-114 Isothermal Extraction. *Anal. Biochem.* **2012**, *424*, 124−126.

(3) Su, W.; Lin, M.; Lee, H.; Cho, M.; Choe, W.-S.; Lee, Y. Determination of Endotoxin through an Aptamer-Based Impedance Biosensor. *Biosens. Bioelectron.* **2012**, *32*, 32−36.

(4) Reich, J.; Tamura, H.; Nagaoka, I.; Motschmann, H. Biologicals Investigation of the Kinetics and Mechanism of Low Endotoxin Recovery in a Matrix for Biopharmaceutical Drug Products. *Biologicals* **2018**, *53*, 1−9.

(5) Zandieh, M.; Hosseini, S. N.; Vossoughi, M.; Khatami, M.; Abbasian, S.; Moshaii, A. Label-Free and Simple Detection of Endotoxins Using a Sensitive LSPR Biosensor Based on Silver Nanocolumns. *Anal. Biochem.* **2018**, *548*, 96−101.

(6) Reich, J.; Lang, P.; Grallert, H.; Motschmann, H. Masking of Endotoxin in Surfactant Samples: Effects on Limulus-Based Detection Systems. *Biologicals* **2016**, *44*, 417−422.

(7) Beutler, B.; Rietschel, E. T. Innate Immune Sensing and Its Roots: The Story of Endotoxin. *Nat. Rev. Immunol.* **2003**, *3*, 169−176.

(8) Konwar, A.; Chowdhury, D.; Dan, A. Chitosan Based *in Situ* and *Ex Situ* Magnetic Iron Oxide Nanoparticles for Rapid Endotoxin Removal from Protein Solutions. *Mater. Chem. Front.* **2019**, *3*, 716−725.

(9) *Biological Tests and Assays.* ⟨*85*⟩ *Bacterial Endotoxins Test 5625*; European Pharmacopoeia and United States Pharmacopeia (USP), 1997.

(10) Klevens, R. M.; Edwards, J. R.; Richards, C. L.; Horan, T. C.; Gaynes, R. P.; Pollock, D. A.; Cardo, D. M. Estimating Health Care-Associated Infections and Deaths in U.S. Hospitals, 2002. *Public Health Rep.* **2007**, *122*, 160−166.

(11) Dales, R.; Miller, D.; Ruest, K.; Guay, M.; Judek, S. Airborne Endotoxin Is Associated with Respiratory Illness in the First 2 Years of Life. *Environ. Health Perspect.* **2006**, *114*, 610−614.

(12) Lim, C.-H.; Yu, I. J.; Kim, H.-Y.; Lee, S.-B.; Kang, M.-G.; Marshak, D. R.; Moon, C.-K. Inflammatory and Immunological Responses to Subchronic Exposure to Endotoxin-Contaminated Metalworking Fluid Aerosols in F344 Rats. *Environ. Toxicol.* **2005**, *20*, 212−218.

(13) Lane, S. R.; Nicholls, P. J.; Sewell, R. D. E. The Measurement and Health Impact of Endotoxin Contamination in Organic Dusts from Multiple Sources: Focus on the Cotton Industry. *Inhalation Toxicol.* **2004**, *16*, 217−229.

(14) Malyala, P.; Singh, M. Endotoxin Limits in Formulations for Preclinical Research. *J. Pharm. Sci.* **2008**, *97*, 2041−2044.

(15) Dobrovolskaia, M. A.; Germolec, D. R.; Weaver, J. L. Evaluation of Nanoparticle Immunotoxicity. *Nat. Nanotechnol.* **2009**, *4*, 411−414.

(16) Balagopal, A.; Gama, L.; Franco, V.; Russell, J. N.; Quinn, J.; Higgins, Y.; Smeaton, L. M.; Clements, J. E.; Thomas, D. L.; Gupta, A. Detection of Microbial Translocation in HIV and SIV Infection Using the Limulus Amebocyte Lysate Assay Is Masked by Serum and Plasma. *PLoS One* **2012**, *7*, No. e41258.

(17) Lourenco, F. R.; Botelho, T. D. S.; Pinto, T. D. J. A. How pH, Temperature, and Time of Incubation Affect False-Positive Responses and Uncertainty of the LAL Gel-Clot Test. *PDA J. Pharm. Sci. Technol.* **2012**, *66*, 542−546.

(18) Liu, F.; Mu, J.; Wu, X.; Bhattacharjya, S.; Yeow, E. K. L.; Xing, B. Peptide-perylene Diimide Functionalized Magnetic Nano-Platforms for Fluorescence Turn-on Detection and Clearance of Bacterial Lipopolysaccharides. *Chem. Commun.* **2014**, *50*, 6200−6203.

(19) Rangin, M.; Basu, A. Lipopolysaccharide Identification with Functionalized Polydiacetylene Liposome Sensors. *J. Am. Chem. Soc.* **2004**, *126*, 5038−5039.

(20) Voss, S.; Fischer, R.; Jung, G.; Wiesmüller, K.-H.; Brock, R. A Fluorescence-Based Synthetic LPS Sensor. *J. Am. Chem. Soc.* **2007**, *129*, 554−561.

(21) Zeng, L.; Wu, J.; Dai, Q.; Liu, W.; Wang, P.; Lee, C. Sensing of Bacterial Endotoxin in Aqueous Solution by Supramolecular Assembly of Pyrene Derivative. *Org. Lett.* **2010**, *12* (18), 4014−4017.

(22) Wu, J.; Zawistowski, A.; Ehrmann, M.; Yi, T.; Schmuck, C. Peptide Functionalized Polydiacetylene Liposomes Act as Fluorescent Turn-On Sensor for Bacterial Lipopolysaccharide. *J. Am. Chem. Soc.* **2011**, *133*, 9720−9723.

(23) Lan, M.; Wu, J.; Liu, W.; Zhang, W.; Ge, J.; Zhang, H.; Sun, J.; Zhao, W.; Wang, P. Copolythiophene-Derived Colorimetric and Fluorometric Sensor for Visually Supersensitive Determination of Lipopolysaccharide. *J. Am. Chem. Soc.* **2012**, *134*, 6685−6694.

(24) Sun, J.; Ge, J.; Liu, W.; Wang, X.; Fan, Z.; Zhao, W.; Zhang, H.; Wang, P.; Lee, S.-T. A Facile Assay for Direct Colorimetric Visualization of Lipopolysaccharides at Low Nanomolar Level. *Nano Res.* **2012**, *5*, 486−493.
(25) Paul, I. E.; Raichur, A. M.; Chandrasekaran, N.; Mukherjee, A. Fluorometric Sensing of Endotoxin Based on Aggregation of CTAB Capped Gold Nanospheres. *J. Lumin.* **2016**, *178*, 106−114.
(26) Liu, T.; Gao, L.; Zhao, J.; Cao, Y.; Tang, Y.; Miao, P. A Polymyxin B-Silver Nanoparticles Colloidal System and the Application of Lipopolysaccharide Analysis. *Analyst* **2018**, *143*, 1053−1058.
(27) Pacheco, M.; Jurado-Sánchez, B.; Escarpa, A. Sensitive Monitoring of Enterobacterial Contamination of Food Using Self-Propelled Janus Microsensors. *Anal. Chem.* **2018**, *90*, 2912−2917.
(28) Gopal, J.; Abdelhamid, H. N.; Hua, P.-Y.; Wu, H.-F. Chitosan Nanomagnets for Effective Extraction and Sensitive Mass Spectrometric Detection of Pathogenic Bacterial Endotoxin from Human Urine. *J. Mater. Chem. B* **2013**, *1*, 2463−2475.
(29) Viraka Nellore, B. P.; Pramanik, A.; Chavva, S. R.; Sinha, S. S.; Robinson, C.; Fan, Z.; Kanchanapally, R.; Grennell, J.; Weaver, I.; Hamme, A. T.; Ray, P. C. Aptamer-Conjugated Theranostic Hybrid Graphene Oxide with Highly Selective Biosensing and Combined Therapy Capability. *Faraday Discuss.* **2014**, *175*, 257−271.
(30) Wang, X.; Han, Q.; Yu, N.; Li, J.; Yang, L.; Yang, R.; Wang, C. Aptamer-Conjugated Graphene Oxide-Gold Nanocomposites for Targeted Chemo-Photothermal Therapy of Cancer Cells. *J. Mater. Chem. B* **2015**, *3*, 4036−4042.
(31) Baker, S. N.; Baker, G. A. Luminescent Carbon Nanodots: Emergent Nanolights. *Angew. Chem., Int. Ed.* **2010**, *49*, 6726−6744.
(32) Luo, P. G.; Sahu, S.; Yang, S.-T.; Sonkar, S. K.; Wang, J.; Wang, H.; LeCroy, G. E.; Cao, L.; Sun, Y.-P. Carbon "Quantum" Dots for Optical Bioimaging. *J. Mater. Chem. B* **2013**, *1*, 2116−2127.
(33) Cao, L.; Wang, X.; Meziani, M. J.; Lu, F.; Wang, H.; Luo, P. G.; Lin, Y.; Harruff, B. A.; Veca, L. M.; Murray, D.; Xie, S.-Y; Sun, Y.-P. Carbon Dots for Multiphoton Bioimaging. *J. Am. Chem. Soc.* **2007**, *129*, 11318−11319.
(34) Lin, Y.; Zheng, Y.; Guo, Y.; Yang, Y.; Li, H.; Fang, Y.; Wang, C. Peptide-Functionalized Carbon Dots for Sensitive and Selective Ca^{2+} Detection. *Sens. Actuators, B* **2018**, *273*, 1654−1659.
(35) Li, H.; Zhang, Y.; Wang, L.; Tian, J.; Sun, X. Nucleic Acid Detection Using Carbon Nanoparticles as a Fluorescent Sensing Platform. *Chem. Commun.* **2011**, *47*, 961−963.
(36) Liu, J.; Li, J.; Jiang, Y.; Yang, S.; Tan, W.; Yang, R. Combination of π -π Stacking and Electrostatic Repulsion between Carboxylic Carbon Nanoparticles and Fluorescent Oligonucleotides for Rapid and Sensitive Detection of Thrombin. *Chem. Commun.* **2011**, *47*, 11321−11323.
(37) Ahmadian-Fard-Fini, S.; Salavati-Niasari, M.; Ghanbari, D. Hydrothermal Green Synthesis of Magnetic Fe_3O_4-Carbon Dots by Lemon and Grape Fruit Extracts and as a Photoluminescence Sensor for Detecting of E. Coli Bacteria. *Spectrochim. Acta, Part A* **2018**, *203*, 481−493.
(38) Liu, Y.; Wang, P.; Shiral Fernando, K. A.; LeCroy, G. E.; Maimaiti, H.; Harruff-Miller, B. A.; Lewis, W. K.; Bunker, C. E.; Hou, Z.-L.; Sun, Y.-P. Enhanced Fluorescence Properties of Carbon Dots in Polymer Films. *J. Mater. Chem. C* **2016**, *4*, 6967−6974.
(39) Liu, X.; Zhang, N.; Bing, T.; Shangguan, D. Carbon Dots Based Dual-Emission Silica Nanoparticles as a Ratiometric Nanosensor for Cu^{2+}. *Anal. Chem.* **2014**, *86*, 2289−2296.
(40) Zhao, X.; Li, M.; Dong, H.; Liu, Y.; Hu, H.; Cai, Y.; Liang, Y.; Xiao, Y.; Zheng, M. Interconnected 3 D Network of Graphene-Oxide Nanosheets Decorated with Carbon Dots for High-Performance Supercapacitors. *ChemSusChem* **2017**, *10*, 2626−2634.
(41) Jia, X.; Li, J.; Wang, E. One-Pot Green Synthesis of Optically pH-Sensitive Carbon Dots with Upconversion Luminescence. *Nanoscale* **2012**, *4*, 5572−5575.
(42) Sun, Y.-P.; Zhou, B.; Lin, Y.; Wang, W.; Fernando, K. A. S.; Pathak, P.; Meziani, M. J.; Harruff, B. A.; Wang, X.; Wang, H.; Luo, P. G.; Yang, H.; Kose, M. E.; Chen, B.; Veca, L. M.; Xie, S.-Y. Quantum-Sized Carbon Dots for Bright and Colorful Photoluminescence. *J. Am. Chem. Soc.* **2006**, *128*, 7756−7757.
(43) Yang, Y.; Kong, W.; Li, H.; Liu, J.; Yang, M.; Huang, H.; Liu, Y.; Wang, Z.; Wang, Z.; Sham, T.-K.; Zhong, J.; Wang, C.; Liu, Z.; Lee, S.-T.; Kang, Z. Fluorescent N-Doped Carbon Dots as *in Vitro* and *in Vivo* Nanothermometer. *ACS Appl. Mater. Interfaces* **2015**, *7*, 27324−27330.
(44) Chandra, S.; Laha, D.; Pramanik, A.; Ray Chowdhuri, A.; Karmakar, P.; Sahu, S. K. Synthesis of Highly Fluorescent Nitrogen and Phosphorus Doped Carbon Dots for the Detection of Fe^{3+} Ions in Cancer Cells: Synthesis of Highly Fluorescent N and P Doped Carbon Dots. *Luminescence* **2016**, *31*, 81−87.
(45) Dong, Y.; Pang, H.; Yang, H. B.; Guo, C.; Shao, J.; Chi, Y.; Li, C. M.; Yu, T. Carbon-Based Dots Co-Doped with Nitrogen and Sulfur for High Quantum Yield and Excitation-Independent Emission. *Angew. Chem., Int. Ed.* **2013**, *52*, 7800−7804.
(46) Xu, Y.; Jia, X.-H.; Yin, X.-B.; He, X.-W.; Zhang, Y.-K. Carbon Quantum Dot Stabilized Gadolinium Nanoprobe Prepared via a One-Pot Hydrothermal Approach for Magnetic Resonance and Fluorescence Dual-Modality Bioimaging. *Anal. Chem.* **2014**, *86*, 12122−12129.
(47) Wang, Y.; Hu, A. Carbon Quantum Dots: Synthesis, Properties and Applications. *J. Mater. Chem. C* **2014**, *2*, 6921−6939.
(48) Luo, R.; Neu, B.; Venkatraman, S. S. Surface Functionalization of Nanoparticles to Control Cell Interactions and Drug Release. *Small* **2012**, *8*, 2585−2594.
(49) Ayyappan, J. P.; Sami, H.; Rajalekshmi, D. C.; Sivakumar, S.; Abraham, A. Immunocompatibility and Toxicity Studies of Poly-L-lysine Nanocapsules in Sprague-Dawley Rats for Drug-Delivery Applications. *Chem. Biol. Drug Des.* **2014**, *84*, 292−299.
(50) Alphandéry, E.; Idbaih, A.; Adam, C.; Delattre, J.-Y.; Schmitt, C.; Guyot, F.; Chebbi, I. Development of Non-Pyrogenic Magnetosome Minerals Coated with Poly-L-lysine Leading to Full Disappearance of Intracranial U87-Luc Glioblastoma in 100% of Treated Mice Using Magnetic Hyperthermia. *Biomaterials* **2017**, *141*, 210−222.
(51) Orive, G.; Tam, S.; Pedraz, J.; Halle, J. Biocompatibility of Alginate-Poly-L-lysine Microcapsules for Cell Therapy. *Biomaterials* **2006**, *27*, 3691−3700.
(52) Anspach, F. B. Endotoxin Removal by Affinity Sorbents. *J. Biochem. Biophys. Methods* **2001**, *49*, 665−681.
(53) Hirayama, C.; Sakata, M.; Nakamura, M.; Ihara, H.; Kunitake, M.; Todokoro, M. Preparation of Poly(ε-lysine) Adsorbents and Application to Selective Removal of Lipopolysaccharides. *J. Chromatogr., Biomed. Appl.* **1999**, *721*, 187−195.
(54) Zhang, Y.; Yu, W.; Han, D.; Meng, J.; Wang, H.; Cao, G. L-lysine Ameliorates Sepsis-Induced Acute Lung Injury in a Lipopolysaccharide-Induced Mouse Model. *Biomed. Pharmacother.* **2019**, *118*, 109307.
(55) Tan, J.; Chen, H.; Gao, Y.; Li, H. Nitrogen-Doped Porous Carbon Derived from Citric Acid and Urea with Outstanding Supercapacitance Performance. *Electrochim. Acta* **2015**, *178*, 144−152.
(56) Sam, S.; Touahir, L.; Salvador Andresa, J.; Allongue, P.; Chazalviel, J.-N.; Gouget-Laemmel, A. C.; Henry de Villeneuve, C.; Moraillon, A.; Ozanam, F.; Gabouze, N.; Djebbar, S. Semiquantitative Study of the EDC/NHS Activation of Acid Terminal Groups at Modified Porous Silicon Surfaces. *Langmuir* **2010**, *26*, 809−814.
(57) Li, X.; Zhang, S.; Kulinich, S. A.; Liu, Y.; Zeng, H. Engineering Surface States of Carbon Dots to Achieve Controllable Luminescence for Solid-Luminescent Composites and Sensitive Be^{2+} Detection. *Sci. Rep.* **2015**, *4*, 4976.
(58) Pallares, R. M.; Su, X.; Lim, S. H.; Thanh, N. T. K. Fine-Tuning of Gold Nanorod Dimensions and Plasmonic Properties Using the Hofmeister Effects. *J. Mater. Chem. C* **2016**, *4*, 53−61.
(59) Kasprzyk, W.; Świergosz, T.; Bednarz, S.; Walas, K.; Bashmakova, N. V.; Bogdał, D. Luminescence Phenomena of Carbon Dots Derived from Citric Acid and Urea - a Molecular Insight. *Nanoscale* **2018**, *10*, 13889−13894.

https://dx.doi.org/10.1021/acsabm.1c00006
ACS Appl. Bio Mater. 2021, 4, 3410−3422

(60) Sciortino, A.; Mauro, N.; Buscarino, G.; Sciortino, L.; Popescu, R.; Schneider, R.; Giammona, G.; Gerthsen, D.; Cannas, M.; Messina, F. β-C_3N_4 Nanocrystals: Carbon Dots with Extraordinary Morphological, Structural, and Optical Homogeneity. *Chem. Mater.* **2018**, *30*, 1695−1700.
(61) Tuerhong, M.; Xu, Y.; Yin, X.-B. Review on Carbon Dots and Their Applications. *Chin. J. Anal. Chem.* **2017**, *45*, 139−150.
(62) Yuan, Y.; Zhang, C.-J.; Gao, M.; Zhang, R.; Tang, B. Z.; Liu, B. Specific Light-Up Bioprobe with Aggregation-Induced Emission and Activatable Photoactivity for the Targeted and Image-Guided Photodynamic Ablation of Cancer Cells. *Angew. Chem., Int. Ed.* **2015**, *54*, 1780−1786.
(63) Wang, J.; Mei, J.; Yuan, W.; Lu, P.; Qin, A.; Sun, J.; Ma, Y.; Tang, B. Z. Hyperbranched Polytriazoles with High Molecular Compressibility: Aggregation-Induced Emission and Superamplified Explosive Detection. *J. Mater. Chem.* **2011**, *21*, 4056−4059.
(64) Gogoi, N.; Agarwal, D. S.; Sehgal, A.; Chowdhury, D.; Sakhuja, R. One-Pot Synthesis of Carbon Nanodots in an Organic Medium with Aggregation-Induced Emission Enhancement (AIEE): A Rationale for "Enzyme-Free" Detection of Cholesterol. *ACS Omega* **2017**, *2*, 3816−3827.
(65) Hu, R.; Lam, J. W. Y.; Liu, J.; Sung, H. H. Y.; Williams, I. D.; Yue, Z.; Wong, K. S.; Yuen, M. M. F.; Tang, B. Z. Hyperbranched Conjugated Poly(Tetraphenylethene): Synthesis, Aggregation-Induced Emission, Fluorescent Photopatterning, Optical Limiting and Explosive Detection. *Polym. Chem.* **2012**, *3*, 1481−1489.
(66) Zhu, L.; Cui, X.; Wu, J.; Wang, Z.; Wang, P.; Hou, Y.; Yang, M. Analytical Methods Fluorescence Immunoassay Based on Carbon Dots as Labels for the Detection of Human Immunoglobulin G. *Anal. Methods* **2014**, *6*, 4430−4436.
(67) Lim, S. K.; Chen, P.; Lee, F. L.; Moochhala, S.; Liedberg, B. Peptide-Assembled Graphene Oxide as a Fluorescent Turn-On Sensor for Lipopolysaccharide (Endotoxin) Detection. *Anal. Chem.* **2015**, *87*, 9408−9412.
(68) Tang, Y.; Kang, A.; Yang, X.; Hu, L.; Tang, Y.; Li, S.; Xie, Y.; Miao, Q.; Pan, Y.; Zhu, D. A Robust OFF-ON Fluorescent Biosensor for Detection and Clearance of Bacterial Endotoxin by Specific Peptide Based Aggregation Induced Emission. *Sens. Actuators, B* **2020**, *304*, 127300.
(69) Wen, L.; Lv, J.; Chen, L.; Li, S.; Mou, X.; Xu, Y. A Fluorescent Probe Composed of Quantum Dot Labeled Aptamer and Graphene Oxide for the Determination of the Lipopolysaccharide Endotoxin. *Microchim. Acta* **2019**, *186*, 122.
(70) Lim, S. Y.; Shen, W.; Gao, Z. Carbon Quantum Dots and Their Applications. *Chem. Soc. Rev.* **2015**, *44*, 362−381.

https://dx.doi.org/10.1021/acsabm.1c00006
ACS Appl. Bio Mater. 2021, 4, 3410−3422